Comparison of printing techniques for the fabrication of flexible carbon nanotube-based ammonia chemiresistive gas sensors

To cite this article: Sahira Vasquez *et al* 2023 *Flex. Print. Electron.* **8** 035012

View the article online for updates and enhancements.

Flexible and Printed Electronics

PAPER

Comparison of printing techniques for the fabrication of flexible carbon nanotube-based ammonia chemiresistive gas sensors

Sahira Vasquez[1], Martina Aurora Costa Angeli[1,*], Mattia Petrelli[1], Mukhtar Ahmad[1], Bajramshahe Shkodra[1], Barbara Salonikidou[2], Radu A Sporea[2], Almudena Rivadeneyra[3], Paolo Lugli[1] and Luisa Petti[1]

1 Sensing Technologies Laboratory (STL), Faculty of Engineering, Free University of Bolzano-Bozen, 39100 Bolzano, Italy
2 Advanced Technology Institute, University of Surrey, Guildford, Surrey, United Kingdom
3 Department of Electronics and Computer Technology, Faculty of Sciences, University of Granada, Granada 18071, Spain
* Author to whom any correspondence should be addressed.

E-mail: martinaaurora.costaangeli@unibz.it

Keywords: dispense printing, screen printing, inkjet printing, carbon nanotubes, chemiresistive sensors, ammonia, printed electronics

Supplementary material for this article is available online

Abstract

Even though a plethora of printing technologies are currently available and their potential for the fabrication of low-cost and flexible sensors has been widely investigated, systematically based, and statistically sustained comparative studies are missing in the literature. In this work, we compare screen, inkjet, and dispense printing for the fabrication of carbon nanotube (CNT)-based ammonia (NH_3) chemiresistive flexible gas sensors for the first time. Moreover, we report the first CNT-based gas sensor fabricated via Voltera printer. The devices were made of a thin layer of spray-coated CNTs and printed silver-based interdigitated electrodes. To draw a thoughtful comparison the same sensor layout, materials, and fabrication flow were used. The device morphological features were acquired through microscopic, atomic force microscope, and 3D images; additionally, the response to NH_3 as well as the printing process characteristics for each technique was analyzed. From 300 μm nominal spacing between lines, we obtained a decrease of 25%, 13%, and 5% on the printed spacings with dispense, screen, and inkjet printing, respectively. At 100 ppm of NH_3, a maximum response of 33%, 31%, and 27% with the dispense-, inkjet-, and screen-printed sensors were found, respectively. Statistical differences were observed between the mean values on the NH_3 response of dispense- compared to the inkjet- and screen-printed sensors, which in effect showed the highest response in the Tukey test. This demonstrated that the fabrication technique employed can induce a different response mainly driven by the printed outcomes. Following a holistic approach that includes the sensor response, the application, the market perspective, and the process versatility, we suggest screen printing as the most suitable method for CNT-based NH_3 gas sensor fabrication.

1. Introduction

In the last decade, several manufacturing technologies have been extensively exploited to fabricate gas sensors, including chemical vapor deposition [1], physical vapor deposition [2], micromachining [3], self-assembly [4], spray coating [5, 6], and printing [7, 8]. Among all, the latter is the most commonly utilized technology for developing miniaturized, portable, and low-cost sensors [9]. Indeed, over

the years, printing technologies (PTs) have diversified, evolved, and advanced, offering the opportunity to realize customized devices, nanoscale features [10], low energy and even low-temperature deposition of more and new functional materials [11] on flexible substrates [12], as well as environmentally friendly or greener processes [13].

Printing is an additive manufacturing technique that follows a bottom-up approach to realize electronic devices by sequentially adding layers of

thickness ranging from the nanometer range [14] to μm [8], depending on the technique. This method substantially reduces the energy consumption and the total fabrication cost, and also it is easy to redesign in comparison with conventional lithographic techniques, where multiple steps are needed for every single layer to be realized [9]. Today many PTs are available, each characterized by different properties such as screen printing, laser direct writing, inkjet printing, soft lithography, flexography, gravure printing, and aerosol printing [8, 15].

Depending on the presence or not of physical contact between the substrate and the material used for the printing (e.g. the ink, the mask), the methods can be classified into two main groups, contact, and non-contact ones. Dispense printing is an example of a non-contact method, in which non-Newtonian highly viscous paste is dispensed continuously onto the substrate through a nozzle with precise volume control, according to the desired layout [16]. Inkjet printing is another example of a non-contact method, however contrary to dispense, here small droplets (1–30 pL) of low-viscous ink are deposited 'drop-on-demand' (DOD) via a micro-nozzle activated by a thermal, piezoelectric or electro-hydrodynamic control by following a digital-based design [17]. On the other hand, screen printing is a typical contact technique characterized by the deposition of a non-Newtonian highly viscous paste through a patterned screen mesh composed of micro-holes [18]. This allows the ink to flow only in the open areas of the screen as the squeegee is pressed over the mesh onto the substrate.

The selection of a PT to fabricate a sensor is driven by the specifications of the method itself, e.g. printing speed, environmental impact, compatibility with the substrate and the functional materials, as well as the device specifications for the final application, such as dimensions, performance, and mechanical properties. However, it is challenging to identify a preferential PT for the fabrication of a specific type of device, such as in the case of chemiresistive gas sensors. These types of sensors are characterized by a relatively straightforward working mechanism; the device resistance changes when the active sensing material is exposed to the target gas [19].

A comprehensive list of the chemiresistive gas sensors realized in the last decades by means of printing can be found in several recent review papers [9, 20–23]. Despite the extensive use of PTs for the realization of chemiresistive gas sensors at a research level, an evaluation of the sensor performance considering the variability associated with these methods (printed outcome compared to the nominal layout) is usually underestimated and not included in such studies. Moreover, the literature lacks standardization in evaluating the device performance that does not allow a simple comparison among the data, making

it challenging to undertake comparative analyses of what has been accomplished and what should be the future directions.

To address the above-mentioned research gap, in this work we have selected two extensively used printing methods (screen printing and inkjet printing) and one less explored technique in gas sensor fabrication (dispense printing) and evaluated the impact of the fully-printed chemiresistive gas sensors performance, by keeping the rest of the major factors constant (type and quantity of sensing material, gas type and concentrations, electrodes layout and material, substrate, gas set up, sensor evaluation criteria and characterization tools). In addition, a holistic approach considering the characteristics and aspects of each method on a lab scale is discussed. For the comparison, ammonia (NH_3) has been selected as the analyte of interest given the importance of its detection. In fact, according to the Occupational Safety and Health Administration, the exposure limit to NH_3 is 35 ppm for 10 min and 25 ppm for 8 h, which makes NH_3 an important hazardous gas [24]. Furthermore, efforts to improve the reliability of NH_3 gas sensors are increasing as the need for NH_3 detection in different areas (e.g. food quality monitoring in intelligent packaging [25], aroma recognition in food [26], food spoilage detection [27] and environmental monitoring [28]) is proportionally increasing.
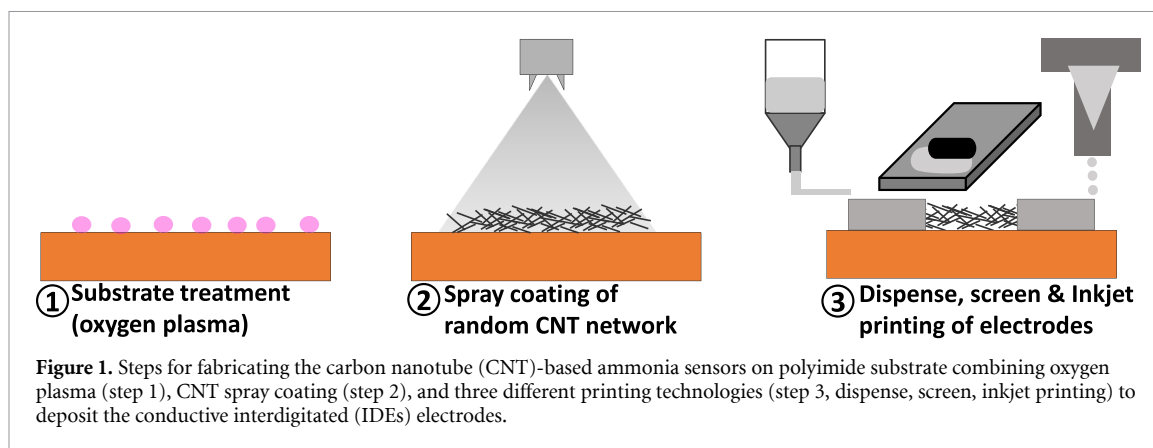
Examples of commonly employed active materials for NH_3-sensors are metal oxide semiconductors [29, 30], conducting polymers [31], 2D materials [32], and carbon nanotubes (CNTs) [33]. In particular, CNTs are among the most widely used functional materials for gas sensor fabrication [34], as they allow the production of low-cost and low-energy demand devices [35, 36] due to their capability of operating at room temperature while showing high sensitivity towards different gas molecules [37] such as NH_3, nitrogen dioxide (NO_2), hydrogen (H_2), methane (CH_4), hydrogen sulfide (H_2S) and sulfur dioxide (SO_2).

In this paper, we discuss the performance of fully printed CNT-based NH_3 gas sensors as a function of three different PTs employed to deposit the electrodes: screen printing, inkjet printing and dispense printing. Spray coating was employed for the deposition of the active material given its feasibility of mass production. This analytical study is especially crucial for CNT-based sensors, given their underlying complex sensing mechanisms where the resolution of the printed patterns bridging the electrodes and the CNT film plays a major role in the device's performance.

2. Materials and methods

2.1. Materials
A flexible 50 μm thick polyimide (PI) foil (Kapton®, from DuPont™) was used as substrate, while high

Figure 1. Steps for fabricating the carbon nanotube (CNT)-based ammonia sensors on polyimide substrate combining oxygen plasma (step 1), CNT spray coating (step 2), and three different printing technologies (step 3, dispense, screen, inkjet printing) to deposit the conductive interdigitated (IDEs) electrodes.

purity ($>$90%) single-walled CNT (P3-SWNT, from Carbon Solutions Inc) as the sensing material. Nitric acid (HNO_3, 65%) and sodium carboxymethyl cellulose (CMC), both from Merck, were employed to create the CNT solution and carry out the sensor post-treatment, respectively. To fabricate the electrodes, a silver (Ag)-based paste (LOCTITE EDAG PF 410 E&C) and a conductive nanosilver ink (Jet-600C) were employed.

2.2. Fabrication process

The proposed CNT-based chemiresistive sensors were completely fabricated using low-cost and versatile PTs, combining spray coating for the CNT deposition and respectively screen, inkjet, and dispense printing for the conductive interdigitated electrodes (IDEs). The fabrication procedure of the printed carbon-based gas sensors presented in this work is schematized in figure 1 and is described below.

2.2.1. Substrate cleaning and pre-treatment

Initially, the PI substrate was ultrasonically cleaned in acetone and then in isopropanol for 5 min. The foil was dried in an oven (Falc Instruments s.r.l) at 200 °C for 24 h. To improve the adhesion to the CNTs, the cleaned foil was exposed to an oxygen plasma treatment [38] (Diener electronics, GmbH & Co. KG) at a constant pressure of 0.4 mbar for 1 min, with a power of 100 W, and 6 cm^3 min^{-1} flow rate [39]. In fact, as previously reported in the literature, oxygen plasma treatment substantially increases CNT attachments due to the formation of polar (i.e. carboxylic) groups on the substrate [40].

2.2.2. CNT dispersion and deposition

CNTs were deposited on the plasma-treated PI by using an air-assisted atomic spray setup (Krautzberger GmbH, Germany) from a water-based dispersion, which was prepared by following the procedure previously described earlier in [41]. Specifically, 0.05% wt CNTs were dispersed in an aqueous CMC solution (0.5% wt) by using an ultrasonic processor (Fisherbrand™ FB-505) at regular intervals of 5 min at 50 % and 30 % power. Subsequently, the solution was centrifuged (Thermo Scientific™ SL 16, equipped with an F15-6 rotor) at 13 000 rpm for 100 min, and the supernatant (ca. 80% of the total solution) was carefully extracted, and stored at room temperature in ambient condition for further use. Before the deposition, the stock solution was diluted (1:15) in deionized water and sonicated in an ultrasonic cleaner (Vetronectina, CP104) for 2 min at 50% power, and 25 °C.

In order to characterize the percolative behavior of the deposited random matrix of the CNT dilution, different layers (where a layer is defined as the complete passage of the spraying gun over the sample area) were sprayed on top of the substrate with the spray coater settings (material flow rate of 4.5, a nozzle to sample distance of 5 cm, a movement speed of 150 mm s^{-1}, and a substrate temperature of 70 °C) (see figure S3). Then, to remove the remaining CMC from the conductive network, the samples were soaked in 2.90 M HNO_3 solution for 1 h, following the optimization reported in [42]. Finally, samples were immersed in DI water for 10 min and dried at 100 °C for 1 h on a hotplate.

2.2.3. Electrodes printing

The IDEs were printed using a dispense, screen, and inkjet printer. A commercial dispense printer (V-One 5000, Voltera) based on a screw motion dispensing unit was used to deposit the Ag paste. The printing settings of the Voltera printer were adjusted to a dispense height of 0.07 mm, a trim length of 150 mm, an anti-stringing distance of 0.1 mm, and a kick of 1.95 mm, as recommended in the literature [43]. For the screen printing process, a semi-automatic screen printing machine (C290, from Aurel automation S.P.A.) equipped with a stainless steel mesh with 125 mesh count per centimeter and a 10 μm of solvent resist over the mesh was used. Finally, the inkjet-printed IDEs were deposited using a Dimatix printer

(DMP-2850, Fujifilm) equipped with a 10 μl cartridge DMC-11610 cartridge. The printing parameters were adjusted according to a drop-to-drop spacing of 30 μm and a plate temperature of 45 °C. Images of the three printing equipment can be found in figure S5.

As a conductive material for the fabrication of IDEs, an Ag-based paste with a viscosity of 17 500 mPas for dispense and screen printing, and a conductive nanosilver ink of 6–10 mPas for inkjet printing was used. The selection of the two types of conductive inks was motivated by the different requirements of the employed PTs. Indeed, screen and dispense techniques are able to deposit shear-thinning thixotropic non-Newtonian' fluids with a viscosity between 5000 and 10 000 cPs [8, 44], whereas inkjet printing can print nanoparticle inks of low viscosity (10–12 cPs), having a particle size 100 times lower than the nozzle diameter to avoid clogging [45]. As a final printing process step, the screen- and dispense-printed IDEs were sintered in the oven at 120 °C for 15 min and the inkjet-printed ones for 25 min, as suggested by the manufacturer datasheet.

PTs are widely known to present systematic differences between nominal and actual layout dimensions, which depend on the chosen technology and set of process parameters. Understanding this layout deviation is paramount when reproducible sensing results are sought, particularly in the field of gas sensors. Thus, the percent of change in the delivered printed outcome of each technology can be used as a parameter to assess the overall printing quality and to evaluate if it ultimately affects the sensor performance. Compared to inkjet and screen printing, dispense printing is the least implemented technology for the fabrication of gas sensors. This motivated the use of the dispense printing to set the design and the nominal dimension of the IDEs employed for all the three PTs here analyzed, as illustrated in table 1. The lowest values of width (W) and spacing (S) to achieve reproducible results in PI were found to be 300 μm and 300 μm, which is consistent with a previous report [43]. Taking into account these limitations and the fact that these values are achievable with all techniques, W and S for all designs were set at 300 and 300 μm, respectively.

2.3. Morphological and electrical characterization
The morphological analysis of both the spray-coated CNT film and the printed IDEs was performed by using an optical microscope (DM8000M, Leica Microsystems CMS GmbH, Wetzlar, Germany) and an atomic force microscope (AFM) from CoreAFM, Nanosurf. The electrical resistance and thickness of the printed IDEs were measured by a portable multimeter (Fluke 287, Everett, WA, USA) and a non-contact 3D optical profilometer (ProFilm3D from Filmetrics, Unterhaching, Germany), respectively.

Table 1. Top-view scheme and nominal dimensions of the IDEs employed to fabricate the printed gas sensors by using screen, inkjet, and dispense printing.

Feature	Nominal value
Line width (W)	300 (μm)
Spacing (S)	300 (μm)
Number of lines	10
Active area	29 (mm^2)
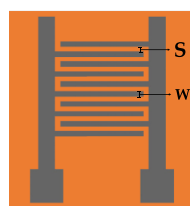
2.4. Sensor characterization
The dispense-, screen-, and inkjet-printed sensor response towards NH_3 was tested in a custom-made gas chamber, automatically controlled with a LabVIEW 2019 program (National Instruments Corporation, Austin, TX, USA). Before initiating the gas test, the sensor was mounted on a module that included a Peltier element for temperature regulation, a PT100 thermoresistor for in-situ temperature monitoring, and connectors for contacting the sensor. The sensor resistance reading was acquired with a digital multimeter (Keithley DAQ6510), while the heating system (Peltier) was powered using a sourcemeter (Keithley 2602B). The sensing cycle consisted of a first step in which the resistance of the sensor at room temperature was recorded in dry air, then a mix of NH_3 gas and air (as carrier gas) was injected for 5 min still at room temperature while maintaining constant the total gas flux (500 ml min^{-1}), and finally, dry air was injected for 15 min at 60 °C and 5 min at room temperature. The heating step was performed to induce an active sensor recovery, causing the release of the gases adsorbed in the film at each exposure [46]. Different NH_3 concentrations (3, 10, 25, 50, and 100 ppm) were injected by diluting the NH_3 gas with air (carrier gas) at room temperature. The complete set up for the data acquisition is illustrated in figure S1.

The sensor performance was evaluated considering the normalized response using the following formula:

$$\text{Normalized Response} = \frac{R_f - R_i}{R_i}, \qquad (1)$$

where R_i is the measured initial resistance of the CNT film before the exposure to a specific NH_3 concentration and R_f is the measured resistance at the end of each exposure cycle.

2.5. Statistical analysis
The effect of the different PTs on the performance of the sensor was evaluated by a completely randomized design composed of a balanced two-factorial arrangement (A × B), where factor A was the effect of the printing method with three levels (dispense, screen, and inkjet), and factor B was the effect of ammonia concentrations with five levels (5, 10, 25, 50, and 100 ppm). Three sensors per each PT were exposed

at each concentration for a total of 45 measurements. Additionally, the effect of factor A on the actual spacing of the IDEs was evaluated. Two-way analysis of variance (ANOVA) was performed using R studio and the differences between the mean values were evaluated by Tukey's HSD (honestly significant difference) test at $p < 0.05$ significance level. The mathematical modeling of the experimental design is described in equation (2):

$$Y_{ijk} = \mu + \alpha_i + \beta_j + \alpha\beta_{ijk} + \epsilon_{ijk}, \qquad (2)$$

where Y_{ijk} = sensor response, i = level of A, j = level of B, k = observation number, μ = general mean, α_i = effect of printing method, β_j = effect of concentration, $(\alpha\beta)_{ij}$ = effect of interaction between printing and concentration, ϵ_{ijk} = experimental error.

3. Results and discussion

3.1. Fabrication process

To deposit a reliable and reproducible thin layer of CNT by spray coating, it is fundamental to optimize the setup parameters (e.g. flow rate, hot plate temperature) [41]. We used AFM to evaluate the reproducibility and the quality of the spray deposition process in terms of a full coverage area of homogeneous bundle-free CNTs, as this is a recommended characteristic that favors resistive sensor performance [34]. Figure 2 shows the AFM micrographs of some of the spray-coated CNT layers (8, 12 and 22) on PI. The images clearly show a homogeneous and bundle-free CNTs distribution with an increase in the surface coverage as the spray layers proportionally increase. Additional information on the spray deposition can be found in figures S2–S4.

The thickness of the Ag line, the geometry, and the actual dimensions compared to the nominal values were analyzed for the three different printed electrodes per technique. The experimental dimension of the sensor layout in a schematic representation and their corresponding microscope images are presented in figure 3. Additional images are provided in figure S6.

The layout deviation with respect to the nominal value (300 μm, for both S and W), indicating a reduction in the case of negative values and an increase in the case of positive, was measured in different points of the Ag line, as highlighted in green, red, and blue colors in figure 3 for dispense-, screen-, and inkjet-printed IDEs, respectively. In the case of the dispense printing, a semi-circular shape at the end of the Ag line was observed, in contrast to the straight lines and sharp edges of the screen and inkjet printed IDEs. These highlighted green circles presented the highest variation in terms of dimension. Therefore,

these measurement locations were excluded, as considered outliers, in the statistical analysis. This feature was consistent for all printings and is related to the specific printing procedure of the dispenser printer [43].

As expected, all the PTs showed a broadening of the line width with respect to the nominal value and a consequent decrease in the spacing. The dispense yielded the highest percentage change in spacing with a decrease of -25%, followed by the screen with -13% and the inkjet with -5%. For the width, the screen showed the highest percentage change with 21%, followed by the dispense with 10%, and finally the inkjet with 6%. It is worth mentioning that, the data extracted from the microscope was highly variable, due to the poor uniformity of the Ag-lines at the microscopic level. This was more pronounced for the dispense-printed lines, where spacings from 90 to 164.5 μm were reached when measuring right at the semi-circular shape. Images of dispense-, screen-, and inkjet-printed sensors can be observed in figures 4(a)–(c).

The ANOVA showed a significant variation among the experimental data of the spacing (S), $p < 0.05$. Tukey's test revealed that dispense and inkjet differed significantly ($p = 0.022$). However, between the screen and dispense there were no statistical differences ($p = 0.066$) as well as between the inkjet and screen ($p = 0.3196$). From the statistical analysis, we can conclude that in terms of layout deviation, the screen showed to be a good trade-off between the dispense and inkjet technologies. Furthermore, even if statistically similar to the screen, inkjet was the technique that offered the closest value to the nominal layout. Indeed, the great capability of the inkjet printer to meet the expected features is what makes this technique the method of choice when looking for precision.

Excluding the semi-circular shape, the screen-printed electrodes showed similar morphology and topography when compared with the dispense-printed ones. Indeed, both had a sandy texture as a consequence of the irregular flake structure of the Ag paste, whereas the inkjet-printed pattern showed a smoother surface typical of Ag nanoparticle-based ink. The different inks used for dispense and screen compared to inkjet printing also determined a different printing thickness of the Ag lines, as shown in the optical profilometer images in figures 4(d)–(f). An average thickness of 10 μm for the dispense- and screen-printed IDEs, and 0.5 μm for the inkjet-printed IDEs was obtained. These values are within the range of those typically reported for screen printed (5–30 μm) and inkjet printed (0.01–0.5 μm) electrodes [20]. The different Ag line thicknesses and conductive inks used affected also the resistance values of the printed Ag lines. We obtained an average
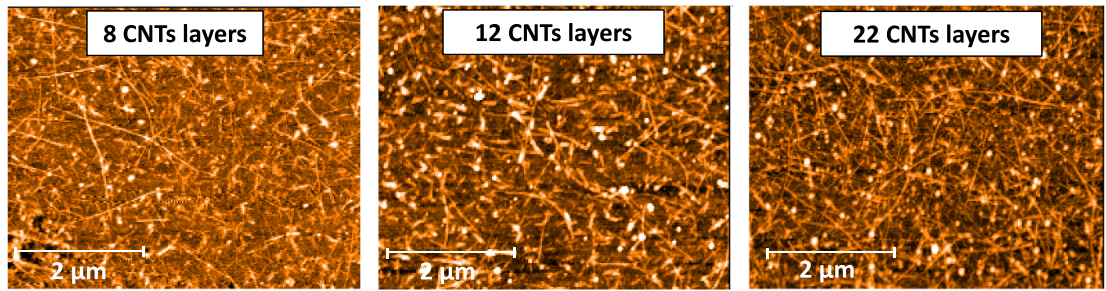
Figure 2. AFM images of 8, 12, and 22 CNT layers spray-coated on polyimide substrate.
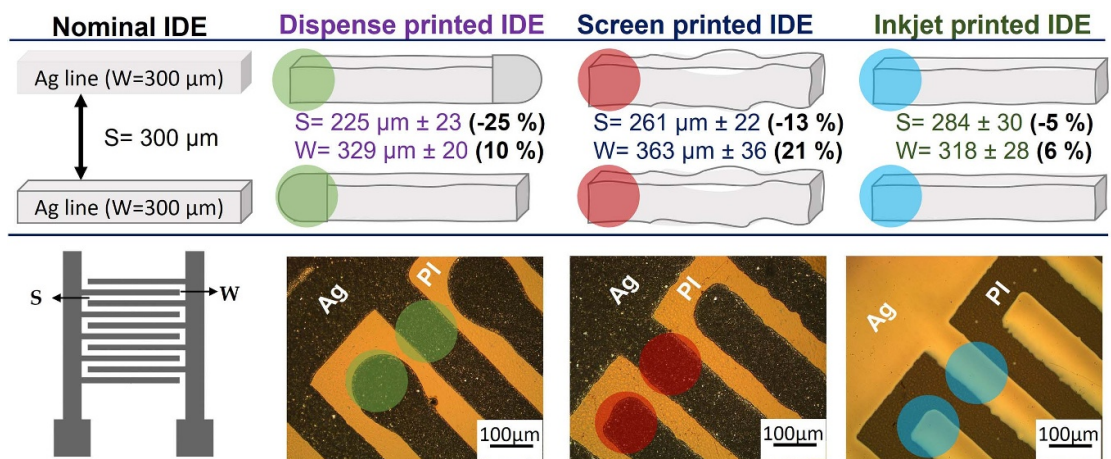

Figure 3. Schematic of the experimental sensor layout's dimensions and the corresponding microscope pictures. The circles in green, red, and blue indicate examples of the measurement reference positions for two parallel Ag lines for each printing.
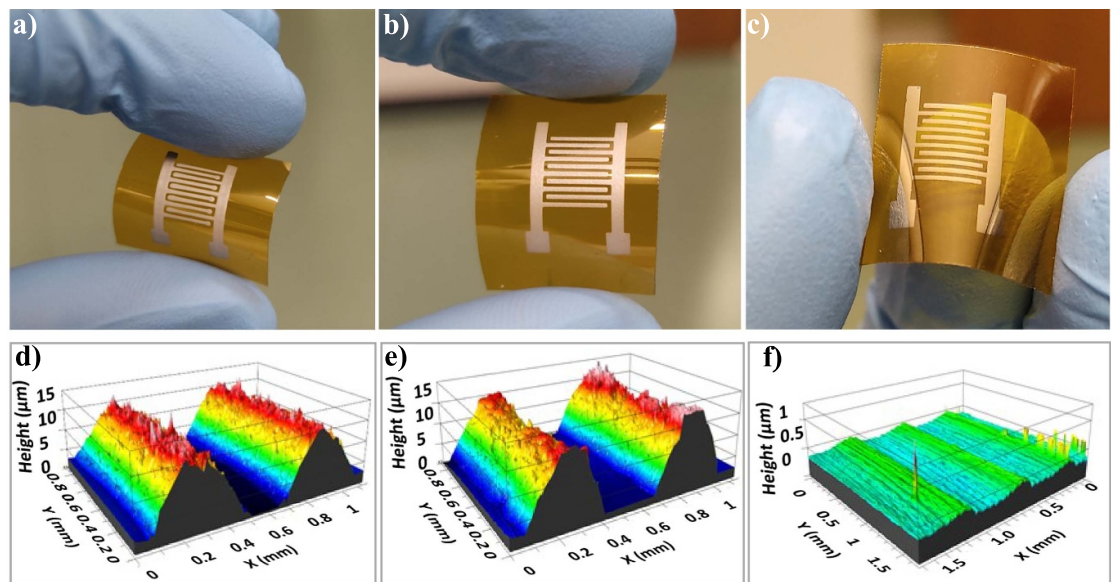

Figure 4. Pictures and profilometer images of: (a) and (d) dispense-printed sensor; (b) and (e) screen-printed sensor; (c) and (f) inkjet-printed sensor.

resistance of 0.21 $\Omega \pm 0.12$ for the dispensed lines, 0.30 $\Omega \pm 0.10$ for the screen ones, and 28.5 $\Omega \pm 3.78$ for the inkjet-printed lines.

Typically, the sensitive layer is deposited on top of the electrodes. However, the length of the CNT used in this work ranges from 0.5 to 1.5 μm, which
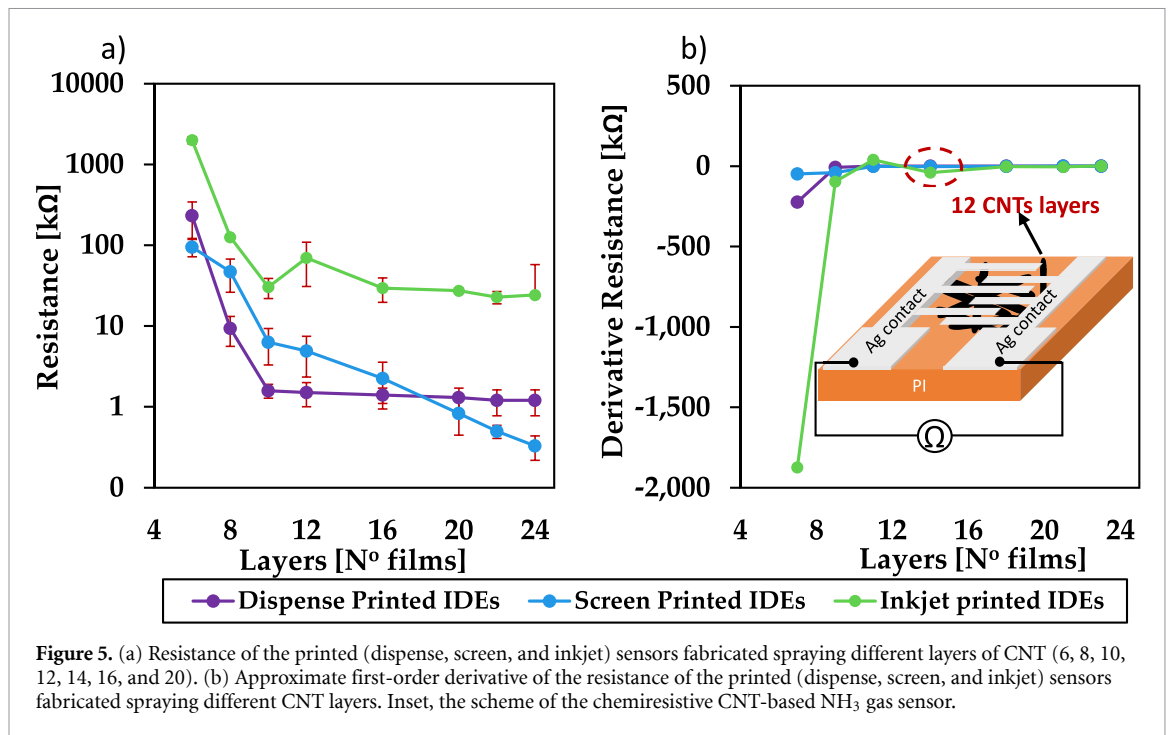
Figure 5. (a) Resistance of the printed (dispense, screen, and inkjet) sensors fabricated spraying different layers of CNT (6, 8, 10, 12, 14, 16, and 20). (b) Approximate first-order derivative of the resistance of the printed (dispense, screen, and inkjet) sensors fabricated spraying different CNT layers. Inset, the scheme of the chemiresistive CNT-based NH_3 gas sensor.

is in the same order of magnitude as the thickness of the inkjet-printed Ag-based electrodes (0.5 μm), and much lower than the dispense- and screen-printed Ag paste electrodes (10 μm). Therefore, to provide a stable and reliable electrical connection between the spray-coated thin film of CNTs and the contact electrode, the IDEs were deposited on top of the CNTs [47], as shown in the inset of figure 5(b). The average resistance of the dispense-, screen-, and inkjet-printed sensors with 6, 8, 10, 12, 14, 16, and 20 layers of spray-coated CNT is shown in figure 5(a). The quantity of the deposited nanomaterial is directly proportional to the number of layers, thus figure 5(a) represents a typical percolative behavior of CNT random networks, where the resistance decreased as the number of layers increased until reaching the percolation threshold. After this value, the ohmic conduction pathway takes over and the resistance remains relatively constant over the increased number of layers.

The percolative threshold of the random CNTs network was experimentally determined by performing the approximate first-order derivative of the curves of resistance versus layers number [48]. As shown in 5(b), up to eight layers there is a high variation in the approximate derivative of the resistance, while the curves reach zero (no more changes in the resistance value by increasing the layer number) at 12 layers. The sensing performance of a CNT-based gas sensor is enhanced when the tube density is within the percolation transition range, being the resistance of the CNT network the most sensitive to any external perturbation in this range. However, in this range, the sensors showed low repeatability and reproducibility [49]. Thus, 12 layers were selected as a compromise
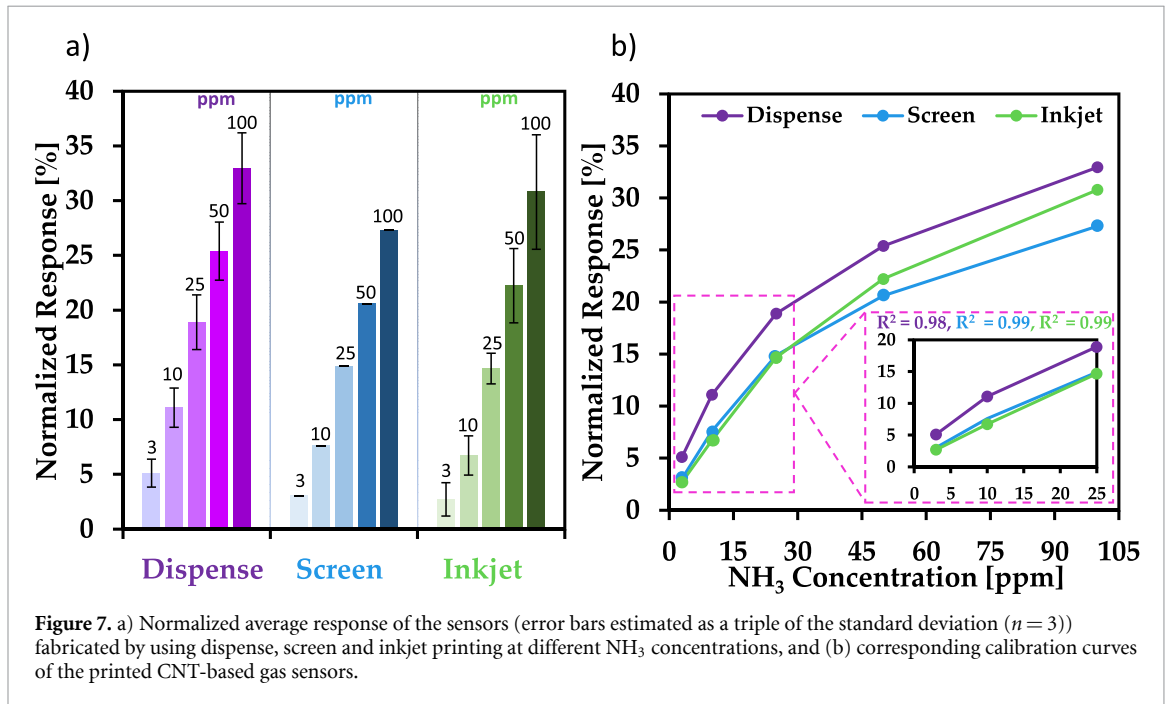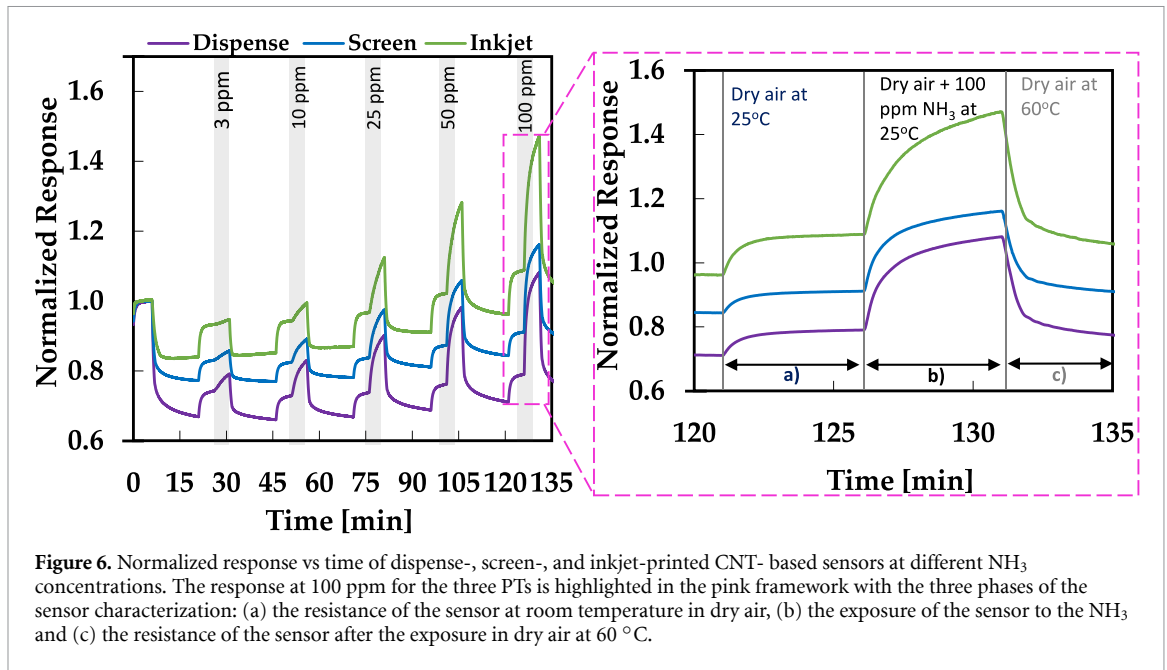
between sensitivity and reproducibility and used to fabricate three sensors for each PT. For this layer number, the average resistance was ca. 1.5 k$\Omega \pm$ 0.5, 4.9 k$\Omega \pm$ 2.6, and 69.75 k$\Omega \pm$ 3.8 for the dispense-, screen- and inkjet-printed IDEs, respectively.

3.2. Characterization of sensors response towards NH_3

The fabricated sensors with the three different printing methods and the 12 CNTs layers were tested for NH_3 detection at the following concentrations 3, 10, 25, 50, and 100 ppm. The resistance was measured as a function of time during the exposure towards NH_3, as presented in the gray bars in figure 6. The 100 ppm exposure cycle is displayed in the pink framework along with the steps carried out during the sensing cycle, as an example of the experimental protocol used for all the reported NH_3 concentrations [35]. The complete set of figures of chemiresistive CNTs-based sensors analyzed per technique in our experiments is provided in figure S7.

Consistently for all the employed PTs, the sensor resistance increased as the NH_3 concentration proportionally increased. This typical behavior of CNT-based sensors in the presence of NH_3 has been extensively studied and reported in the literature [50, 51]. Briefly, the adsorption of NH_3 onto the CNT layer causes an electron transfer that involves intratube and intertube modulation. Specifically, NH_3 donates electrons to the valence band of the CNT network reducing hole density in the as-prepared p-type CNT film and thus increasing the electrical resistance.

As expected, this well-known CNT sensing mechanism in the presence of NH_3 was similar across

Figure 6. Normalized response vs time of dispense-, screen-, and inkjet-printed CNT- based sensors at different NH_3 concentrations. The response at 100 ppm for the three PTs is highlighted in the pink framework with the three phases of the sensor characterization: (a) the resistance of the sensor at room temperature in dry air, (b) the exposure of the sensor to the NH_3 and (c) the resistance of the sensor after the exposure in dry air at 60 °C.

Figure 7. a) Normalized average response of the sensors (error bars estimated as a triple of the standard deviation ($n = 3$)) fabricated by using dispense, screen and inkjet printing at different NH_3 concentrations, and (b) corresponding calibration curves of the printed CNT-based gas sensors.

the three different sensors independently of the PTs, as shown in figure 7(a). The corresponding calibration curves presented in figure 7(b), demonstrate a linear behavior with increasing concentration up to about 25 ppm, similar to the results previously reported in [51]. Nevertheless, within the tested range (3–100 ppm), a large response up to 33% was obtained, demonstrating the high sensitivity and strong affinity of CNT towards NH_3, independently of the PTs. As mentioned in the introduction, the exposure limit to NH_3 is 35 ppm for 10 min and 25 ppm for 8 h [24]. Therefore, the sensors presented here can be used for NH_3 monitoring, considering that within

this range all sensors exhibited high sensitivity and good linearity.

Table 2 shows a summary containing the main features of the different fully printed sensors, for the lowest (3 ppm) and highest (100 ppm) NH_3 concentration tested. The dispense-printed sensors showed the highest response as well as the best sensor linearity, followed by the inkjet-and screen-printed ones.

To evaluate if these results were statistically significant, a statistical analysis was performed. The ANOVA showed that there was a significant main effect between factor A (printing, $p < 0.001$) and B (concentrations, $p < 0.001$), but no interactive effect

Table 2. Summary of the performance of the dispense, screen, and inkjet printed NH_3 sensors.

Parameter	Dispense printing	Screen printing	Inkjet printing
Response ($\Delta R/Ro$) at 100 ppm %	33 ± 4	27 ± 1	31 ± 5
Response ($\Delta R/Ro$) at 3 ppm %	5 ± 2	3 ± 1	3 ± 2
Sensitivity[a]/Linearity (R^2)	0.61/0.98	0.53/0.99	0.54/0.99

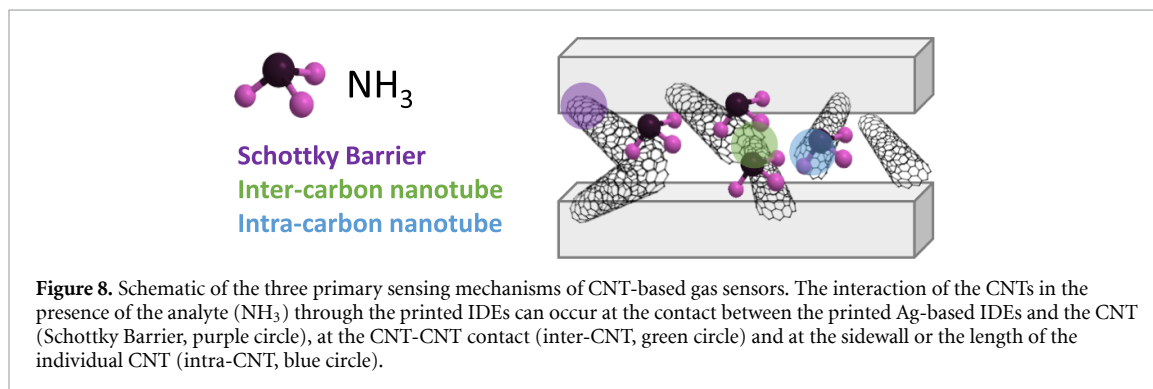[a] Slope of the linear fitting of the curve from 3 up to 25 ppm.

Figure 8. Schematic of the three primary sensing mechanisms of CNT-based gas sensors. The interaction of the CNTs in the presence of the analyte (NH_3) through the printed IDEs can occur at the contact between the printed Ag-based IDEs and the CNT (Schottky Barrier, purple circle), at the CNT-CNT contact (inter-CNT, green circle) and at the sidewall or the length of the individual CNT (intra-CNT, blue circle).

($p = 0.088$), which means that printing and concentrations are independent of each other and can be analyzed separately. To simplify the analysis, we have focused on the printing factor. For this, the Tukey test showed that the screen- and inkjet-printed sensors response was not significantly different ($p = 0.73$), however, the response of the dispense-printed sensor differed significantly ($p > 0.05$) from the other two sensor groups. In fact, dispense-printed sensors showed the highest response.

The sensor response towards NH_3 can be explained by considering that the PT affected the trace thickness, profile shape, edge, and sample-to-sample variability. In particular, the layout deviation with respect to the nominal value is consequently influencing the performance of the sensors. The most notable difference between the three different printed patterns was the presence of a semicircular shape at the end of the Ag line of the dispense printed sensors which in effect decreased considerably the spacing (90–164 μm). Thus, we believe that the achieved narrow spacing (not considered in the statistical analysis of the spacing presented in section 3.1) tuned the overall sensor response towards higher values. The broadening of the electrodes and decreased spacing in these points might have, in fact, enhanced the lateral fringing effect, contributing to the increase in the response of the dispense printed sensor. In this respect, future experiments will include the evaluation of such phenomenon, by performing simulations and by limiting the deposition of the film to the internal part of the IDEs, to ensure that the semicircular shape at the end of the Ag line is not in contact with the CNT thin film.
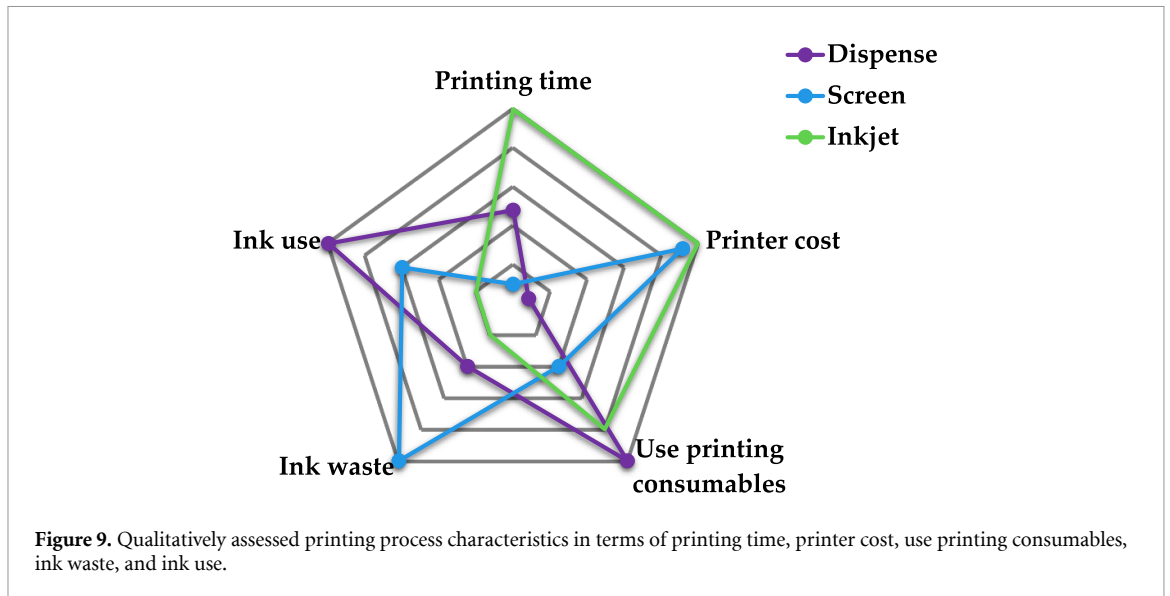
Indeed, even if the sensing mechanism of CNT-based sensors is very complex (dominated by one of

Table 3. Irreversibility values of the different printed sensors.

Concentration (ppm)	Dispense printed (%)	Screen printed (%)	Inkjet printed (%)
3–10	-0.59 ± 0.83	0.86 ± 2.64	1.46 ± 2.18
10–25	1.20 ± 0.96	2.65 ± 2.07	2.23 ± 1.03
25–50	2.67 ± 1.95	4.50 ± 2.70	4.00 ± 1.31
50–100	2.84 ± 2.06	4.95 ± 2.85	4.26 ± 1.40

the three sensing mechanisms or maybe a combination of them: intra-tubes, Schottky Barrier, and intertube, as depicted in figure 8, and still not fully understood, it is well-accepted that the primary sensing mechanisms rely on semiconductive intertube modulation and so it is affected by the percolative film [36, 52]. Since the quantity of semiconducting pathway is depending on the IDE spacing [53], the PT used is ultimately influencing the response of the sensors. Thus, we believe that in our specific case, the resulting response was impacted by the reduced spacing achieved with the dispense PT in specific spots of the active area.

The average irreversibility and the standard deviation calculated by comparing the resistance following each exposure cycle with the previous initial resistance for the three different printed sensors is presented in table 3. The graphical representation of this parameter and the corresponding equation is provided in figure S8. The drift and irreversibility are undesirable features for practical sensors and are still major problems of CNT-based sensors [54]. At low concentrations for the three printed sensors, the irreversibility is below 2.65%, while at high concentrations, the percentage, particularly for the inkjet and screen printed sensor, is above 4%. The table also

Figure 9. Qualitatively assessed printing process characteristics in terms of printing time, printer cost, use printing consumables, ink waste, and ink use.

demonstrates that like for the other sensing parameters the dispense printed sensor performed better, showing the lowest percentage at both low and high gas concentrations. More investigations to further explore this aspect will be performed in future experiments.

The sensitivity of CNTs to a variety of environmental stimuli (such as RH, temperature, pressure, and gases) is well recognized. Although the impact of these conditions, except for NH_3 was not assessed in our investigation, this aspect will be taken into account for subsequent trials. However, regardless of how these factors affected the CNTs surface, all sensors were tested in identical ambient conditions. Therefore, the impact is similar across all printed sensors. Furthermore, it should be highlighted that even if dispense-printed sensors showed the highest sensitivity, lowest irreversibility, and better linearity, the screen-printed sensors showed the lowest standard deviation. This can be attributed both to the fact that screen printing is a more repeatable technique as well as to the physical contact of the screen during printing favoring a better electrical contact, making this response more stable and less noisy and therefore more consistent between samples. This confirms the capability of the screen PT to produce reproducible and robust sensors as demonstrated in [55].

3.3. Lab scale printing process analysis

In order to fully evaluate and compare the PTs, it is not enough to limit the discussion to the sensing performance of the final devices, as this needs to cover also the overall production process's feasibility, complexity, and cost. For this purpose, a qualitative assessment of the printing process to a lab scale was performed considering several processing criteria, as illustrated in figure 9. In the graph, the three PTs are

analyzed based on their: printing time, printer cost, use of printing consumables, ink waste, and ink use. Dispense printing has the advantages of low printer cost and ink waste, but high ink use (required for the calibration step). The ink waste was happening during the calibration step, once the calibration was done, the ink was deposited precisely via a nozzle only when needed and the remaining material on the cartridge was stored for further use. In addition, dispense printing requires high variability of consumables per printing (disposable and plastic nozzles, pistons, and empty clear cartridges). To print 12 sensors, 24 min were required, offering an average time compared to the other two techniques. Screen printing, while requiring low printing time (5 min to print 12 sensors) and consumables use per printing due to the highly automated parts and simple printing steps through contact, it produced a high ink waste (due to the left material inside the mesh and the constant cleaning of the screen needed between printing to avoid the clogging of the mesh) while presenting a high printer cost. Additionally, any modification of the design requires the purchase of a new mask while the other two techniques rely on digital design modifications. Finally, inkjet printing offered the advantages of very low ink use and waste, thanks to the capability to deposit a few picoliters of material DOD but required the highest printing time (50 min to print 12 sensors) a low printing speed, and longer post-treatment.

4. Conclusion

This work presents a systematic experimental-based comparative analysis between CNT-based NH_3 sensors fabricated by using dispense, screen, and inkjet PTs. The CNT sensing layer was deposited

via spray coating on a flexible PI substrate and the dispense, screen, and inkjet PTs were employed to deposit the Ag-based IDEs. The different PTs were compared in terms of morphological features, the gas-sensing performance of the so fabricated sensors, and the fabrication processes in terms of material used, time, and printer cost. The dispense-PT showed to be a highly versatile prototyping fabrication method resulting in the highest variability on the actual dimension of the printed design, which however yielded the highest NH_3 sensing response. On the other hand, screen-printed sensors showed the best reproducibility in the gas sensor response in terms of the lowest standard deviation and the higher production rate, while inkjet-printing proved to be the technique that allows the lowest ink waste with fabrication reproducibility and sensing performance in between the screen and dispense printing. All our findings were supported by a meticulous statistical analysis, by means of ANOVA and Tukey tests, after carefully selecting and considering all the process parameters. Considering all the findings, we selected screen printing as the most suitable method for CNT-based NH_3 gas sensor fabrication, due to the provided high reproducibility, large-scale fabrication, and good sensor response. To conclude, the influence of the dimension and morphology of the contacts connecting the CNTs and the uniformity of the conductive layer is investigated. The comparison of three PTs for the fabrication of printed NH_3 gas sensors in a systematic manner as compared to the state of the art on printed CNTs-based sensors is provided. Furthermore, the results of the printed patterns can also be used to predict future outcomes when utilizing similar PTs. Future work will be focused on the evaluation of the influence of the deposition techniques and process parameters for the sensing materials, i.e. CNT ink, and the improvement of the sensing performance, with respect to selectivity, irreversibility, and influence of the environmental conditions.

Data availability statement

All data that support the findings of this study are included within the article (and any supplementary files).

Acknowledgments

ORCID iDs

Sahira Vasquez https://orcid.org/0000-0001-5213-3890
Martina Aurora Costa Angeli https://orcid.org/0000-0002-9302-4292
Mattia Petrelli https://orcid.org/0000-0002-0416-0904
Mukhtar Ahmad https://orcid.org/0000-0001-8514-2718
Bajramshahe Shkodra https://orcid.org/0000-0002-2414-8590
Barbara Salonikidou https://orcid.org/0000-0001-7922-061X
Radu A Sporea https://orcid.org/0000-0002-3759-3255
Almudena Rivadeneyra https://orcid.org/0000-0001-8133-1992
Paolo Lugli https://orcid.org/0000-0002-2511-5643
Luisa Petti https://orcid.org/0000-0003-0264-7185

References

[1] Gautam M and Jayatissa A H 2011 *Mater. Sci. Eng.* C **31** 1405–11
[2] Rossnagel S 2003 *J. Vac. Sci. Technol.* A **21** S74–S87
[3] Simon I, Barsan N, Bauer M and Weimar U 2001 *Sens. Actuators* B **73** 1–26
[4] Wang Y, Zhang L, Hu N, Wang Y, Zhang Y, Zhou Z, Liu Y, Shen S and Peng C 2014 *Nanoscale Res. Lett.* **9** 1–12
[5] Abdellah A, Abdelhalim A, Loghin F, Kohler P, Ahmad Z, Scarpa G and Lugli P 2013 *IEEE Sens. J.* **13** 4014–21
[6] Loghin F, Colasanti S, Weise A, Falco A, Abdelhalim A, Lugli P and Abdellah A 2016 *Flex. Print. Electron.* **1** 045002
[7] Ru C, Luo J, Xie S and Sun Y 2014 *J. Micromech. Microeng.* **24** 053001
[8] Angeli M A C, Ciocca M, Petti L and Lugli P 2021 Advances in printing technologies for soft robotics devices applications *Advances in Chemical Engineering* vol 57 (Elsevier) pp 45–89
[9] Dai J, Ogbeide O, Macadam N, Sun Q, Yu W, Li Y, Su B L, Hasan T, Huang X and Huang W 2020 *Chem. Soc. Rev.* **49** 1756–89
[10] Chen S, Su M, Zhang C, Gao M, Bao B, Yang Q, Su B and Song Y 2015 *Adv. Mater.* **27** 3928–33
[11] Bernasconi R, Angeli M C, Mantica F, Carniani D and Magagnin L 2019 *Polymer* **185** 121933
[12] Angeli M A C, Caronna F, Cramer T, Gastaldi D, Magagnin L, Fraboni B and Vena P 2019 *IEEE Sens. J.* **20** 4087–95
[13] Guna V K, Murugesan G, Basavarajaiah B H, Ilangovan M, Olivera S, Krishna V and Reddy N 2016 *IEEE Trans. Electron Devices* **63** 4893–8
[14] Salonikidou B, Mehonic A, Takeda Y, Tokito S, England J and Sporea R A 2022 *Adv. Eng. Mater.* **24** 2200439
[15] Rivadeneyra A, Loghin F C and Falco A 2018 Technological integration in printed electronics *Flexible Electronics* (IntechOpen)
[16] Shen A, Caldwell D, Ma A W and Dardona S 2018 *Additive Manuf.* **22** 343–50
[17] He B, Yang S, Qin Z, Wen B and Zhang C 2017 *Sci. Rep.* **7** 1–7
[18] Khan S, Lorenzelli L and Dahiya R S 2014 *IEEE Sens. J.* **15** 3164–85
[19] Jian Y, Hu W, Zhao Z, Cheng P, Haick H, Yao M and Wu W 2020 *Nano-Micro Lett.* **12** 1–43

[20] Fioravanti A and Carotta M C 2020 *Appl. Sci.* **10** 1741

[21] Pandhi T, Chandnani A, Subbaraman H and Estrada D 2020 *Sensors* **20** 5642

[22] Kumar S, Pavelyev V, Tripathi N, Platonov V, Sharma P, Ahmad R, Mishra P and Khosla A 2020 *J. Electrochem. Soc.* **167** 047506

[23] Alrammouz R, Podlecki J, Abboud P, Sorli B and Habchi R 2018 *Sens. Actuators* A **284** 209–31

[24] Kwak D, Lei Y and Maric R 2019 *Talanta* **204** 713–30

[25] Schweizer-Berberich P M, Vaihinger S and Göpel W 1994 *Sens. Actuators* B **18** 282–90

[26] Aishima T 1991 *J. Agric. Food Chem.* **39** 752–6

[27] Matindoust S, Farzi A, Baghaei Nejad M, Shahrokh Abadi M H, Zou Z and Zheng L R 2017 *J. Mater. Sci., Mater. Electron.* **28** 7760–8

[28] Afshar-Mohajer N, Zuidema C, Sousan S, Hallett L, Tatum M, Rule A M, Thomas G, Peters T M and Koehler K 2018 *J. Occup. Environ. Hygiene* **15** 87–98

[29] Zappa D, Galstyan V, Kaur N, Munasinghe Arachchige H M, Sisman O and Comini E 2018 *Anal. Chim. Acta* **1039** 1–23

[30] Nunes D, Pimentel A, Gonçalves A, Pereira S, Branquinho R, Barquinha P, Fortunato E and Martins R 2019 *Semicond. Sci. Technol.* **34** 043001

[31] Yu S H, Cho J, Sim K M, Ha J U and Chung D S 2016 *ACS Appl. Mater. Interfaces* **8** 6570–6

[32] Mao S, Chang J, Pu H, Lu G, He Q, Zhang H and Chen J 2017 *Chem. Soc. Rev.* **46** 6872–904

[33] Goldoni A, Petaccia L, Lizzit S and Larciprete R 2009 *J. Phys.: Condens. Matter* **22** 013001

[34] Zhang W D and Zhang W H 2009 *J. Sens.* **2009** 160698

[35] Abdellah A, Abdelhalim A, Horn M, Scarpa G and Lugli P 2013 *IEEE Trans. Nanotechnol.* **12** 174–81

[36] Abdellah A, Abdelhalim A, Loghin F, Köhler P, Ahmad Z, Scarpa G and Lugli P 2013 *IEEE Sens. J.* **13** 4014–21

[37] Schroeder V, Savagatrup S, He M, Lin S and Swager T M 2018 *Chem. Rev.* **119** 599–663

[38] Cen-Puc M, Schander A, Vargas Gleason M G and Lang W 2021 *Polymers* **13** 1955

[39] Shkodra B, Demelash Abera B, Cantarella G, Douaki A, Avancini E, Petti L and Lugli P 2020 *Biosensors* **10** 35

[40] Bouhamed A, Choura S and Kanoun O 2016 *NANOCON 2016—Conf. Proc., 8th Int. Conf. on Nanomaterials—Research and Application* pp 42–47

[41] Shkodra B, Petrelli M, Angeli M A C, Inam A S, Lugli P and Petti L 2022 *IEEE Sens. J.* 1–8

[42] Loghin F, Rivadeneyra A, Becerer M, Lugli P and Bobinger M 2019 *Nanomaterials* **9** 471

[43] Vasquez S, Petrelli M, Angeli M C, Costa J, Avancini E, Cantarella G, Munzenrieder N, Lugli P and Petti L 2021 *2021 5th IEEE Electron Devices Technology and Manufacturing Conf., EDTM 2021* pp 2–4

[44] Kim J, Kumar R, Bandodkar A J and Wang J 2017 *Adv. Electron. Mater.* **3** 1600260

[45] Lee A, Sudau K, Ahn K H, Lee S J and Willenbacher N 2012 *Indus. Eng. Chem. Res.* **51** 13195–204

[46] Falco A, Rivadeneyra A, Loghin F, Salmeron J, Lugli P and Abdelhalim A 2018 *J. Mater. Chem.* A **6** 7107–13

[47] Abdelhalim A, Falco A, Loghin F, Lugli P, Salmerón J F and Rivadeneyra A 2016 Flexible nh3 sensor based on spray deposition and inkjet printing *2016 IEEE Sensors* pp 1–3

[48] Rahaman M, Aldalbahi A, Govindasami P, Khanam N P, Bhandari S, Feng P and Altalhi T 2017 *Polymers* **9** 527

[49] Wang Y and Yeow J T 2009 *J. Sens.* **2009** 1–24

[50] Zhao J, Buldum A, Han J and Lu J P 2002 *Nanotechnology* **13** 195–200

[51] Loghin F C, Bobinger M, Rivadeneyra A, Becerer M and Lugli P 2019 Flexible carbon nanotube sensors with screen printed and interdigitated electrodes *2019 IEEE 19th Int. Conf. on Nanotechnology (IEEE)* pp 1–4

[52] Boyd A, Dube I, Fedorov G, Paranjape M and Barbara P 2014 *Carbon* **69** 417–23

[53] Loghin F C, Falco A, Salmeron J F, Lugli P, Abdellah A and Rivadeneyra A 2019 *Sensors* **19** 4591

[54] Fennell Jr J F, Liu S F, Azzarelli J M, Weis J G, Rochat S, Mirica K A, Ravnsbæk J B and Swager T M 2016 *Angew. Chem., Int. Edn* **55** 1266–81

[55] White N M and Turner J D 1997 *Meas. Sci. Technol.* **8** 1–20